Nuclear Science and Techniques (2024) 35:143
https://doi.org/10.1007/s41365-024-01531-0

Direct measurement of the break-out ^{19}F(p, γ)^{20}Ne reaction in the China Jinping underground laboratory (CJPL)

Yin-Ji Chen[1] · Hao Zhang[1] · Li-Yong Zhang[1,11] · Jian-Jun He[1,12] · Richard James deBoer[2] · Michael Wiescher[2] · Alexander Heger[3] · David Kahl[4] · Jun Su[1,11] · Daniel Odell[5] · Xin-Yue Li[1] · Jian-Guo Wang[6] · Long Zhang[7] · Fu-Qiang Cao[7] · Zhi-Cheng Zhang[8] · Xin-Zhi Jiang[1] · Luo-Huan Wang[1,13] · Zi-Ming Li[1] · Lu-Yang Song[1] · Liang-Ting Sun[6,9] · Qi Wu[6] · Jia-Qing Li[6] · Bao-Qun Cui[7] · Li-Hua Chen[7] · Rui-Gang Ma[7] · Er-Tao Li[8] · Gang Lian[7] · Yao-De Sheng[1] · Zhi-Hong Li[7] · Bing Guo[7] · Wei-Ping Liu[7,10]

Received: 3 February 2024 / Revised: 10 May 2024 / Accepted: 13 May 2024

Abstract
Calcium production and the stellar evolution of first-generation stars remain fascinating mysteries in astrophysics. As one possible nucleosynthesis scenario, break-out from the hot carbon–nitrogen–oxygen (HCNO) cycle was thought to be the source of the calcium observed in these oldest stars. However, according to the stellar modeling, a nearly tenfold increase in the thermonuclear rate ratio of the break-out ^{19}F(p, γ)^{20}Ne reaction with respect to the competing ^{19}F(p,α)^{16}O back-processing reaction is required to reproduce the observed calcium abundance. We performed a direct measurement of this break-out reaction at the China Jinping underground laboratory. The measurement was performed down to the low-energy limit of $E_{\mathrm{c.m.}} = 186$ keV in the center-of-mass frame. The key resonance was observed at 225.2 keV for the first time. At a temperature of approximately 0.1 GK, this new resonance enhanced the thermonuclear ^{19}F(p, γ)^{20}Ne rate by up to a factor of ≈ 7.4, compared with the previously recommended NACRE rate. This is of particular interest to the study of the evolution of the first stars and implies a stronger breakdown in their "*warm*" CNO cycle through the ^{19}F(p, γ)^{20}Ne reaction than previously envisioned. This break-out resulted in the production of the calcium observed in the oldest stars, enhancing our understanding of the evolution of the first stars.

Keywords Nuclear astrophysics · First stars · Abundance of calcium · Reaction cross section · Reaction rate · China Jinping underground laboratory (CJPL) · JUNA

1 Introduction

Stars are responsible for creating elements heavier than helium. The first generation of stars, also called Population III (Pop III) stars or primordial stars, were formed from primordial matter (mainly H and He) left behind by the Big Bang. These first stars play a special role in seeding the universe with the first metals and in creating suitable conditions for future generations of stars.

The first stars were predominantly very massive and spent the majority of their lives quiescently fusing hydrogen into helium in their cores through catalytic carbon–nitrogen–oxygen (CNO) cycles, where carbon was produced in the previous triple alpha process or the sequential alpha capture mechanism [1–4]. As a catalytic reaction, the net CNO mass fraction remains constant unless a break-out reaction sequence causes a leak toward the NeNa mass region or the temperature and density are high enough to forge new carbon by the triple alpha (3α) process, as is the case for primordial massive stars. A leak via the ^{19}F(p, γ)^{20}Ne reaction causes an irreversible flow from the CNO to the NeNa region because none of the (p, α) feedback processes via Ne isotopes are energetically possible [5]. For materials that leak through fluorine, protons capture and decay along the stability valley, leading

This work was supported by the National Natural Science Foundation of China (Nos. 12075027, 1232509, 11961141004, and 12175152) and the National Science Foundation (Nos. Phys-2011890 and Phy-1430152).

Extended author information available on the last page of the article

to the production of a double magic nucleus ^{40}Ca [6–8]. The leakage depends on the thermonuclear rate ratio of the break-out ^{19}F(p,γ)^{20}Ne reaction and the competing back-processing ^{19}F(p, α)^{16}O reaction.

Previously, the (p, γ) reaction was assumed to be extremely weak compared with the competing (p, α) reaction, and models predicted that most of the ^{19}F produced by the CNO cycle would be recycled back into ^{16}O without significant changes in chemical abundance [9]. This assumption was made by simply extrapolating the high-energy cross section data of ^{19}F(p, γ)^{20}Ne down to the region of astrophysical interest, which can introduce large uncertainties, as shown in the present work, due to the absence of low-energy resonances [10]. In contrast, the (p, α) rate was determined with more reliable experimental data because of its larger cross section [11–13]. It was pointed out that if this ratio was approximately 10 times larger than the currently adopted value, the observed Ca abundance at the oldest star, SMSS0313-6708, could be reproduced by the stellar models [7].

Despite the importance of the ^{19}F(p, γ)^{20}Ne reaction, experimental data within the Gamow window ($E_{\mathrm{c.m.}}$ = 76–146 keV) of Pop III stars' hydrogen-burning temperatures (~ 0.1 GK) are notably lacking due to the extremely low cross section of the ^{19}F(p, γ)^{20}Ne reaction at low energy. Previous experimental studies focused mainly on the energy range of $E_{\mathrm{c.m.}}$ > 300 keV, where the absolute cross section is higher [10, 14–20]. Even in this high-energy region, experimental data remain scarce, primarily because of the intricate challenges posed by the strong 6130 keV γ-ray background originating from the ^{19}F(p,$\alpha\gamma$)^{16}O reaction.

Some early measurements used low-resolution and relatively small-volume NaI(TI) detectors to measure the > 11 MeV γ rays emitted from the primary transition to the first excited state of ^{20}Ne (see Fig. 1) [14–17]. However, the energy resolution was insufficient to separate the primary transition γ rays from the 12.26 MeV pileup peak of the ^{19}F(p,$\alpha\gamma$)^{16}O reaction; thus, large uncertainties may still exist. Here, the 12.26-MeV pileup peak originated from the 6130-keV γ rays (i.e., 'γ_2' in Fig. 1) produced by the ^{19}F(p, $\alpha\gamma$)^{16}O reaction, whose cross section is (~ 1000 times larger than that of the (p, γ) channel of present interest. When two 6130-keV γ rays are detected simultaneously within a single time window, a pileup peak around 12.26 MeV is produced. Subsequent advancements, such as the use of high-resolution Ge(Li) detectors, have provided improved measurement results, such as those by Subotic et al. [18] and Clifford [19]. However, detection limitations and uncertainties persist owing to low efficiency and restricted energy ranges. In Subotic et al., 24 cm^3 and 36 cm^3 Ge(Li) detectors and a 7.6 cm × 7.6 cm NaI(Tl) crystal were used to measure the excitation functions and angular distribution. It should be noted that the angular distribution was only measured for the resonance E_{p} = 1091 keV. Because of its low detection efficiency, this measurement was limited to the on-resonance region of E_{p} = 340–935 keV, which is much higher than the $E_{\mathrm{c.m.}}$ = 76–146 keV Gamow window of Pop III stars in the hydrogen-burning stage. Clifford's measurement is similar to that of Subotic et al., but is limited to an even higher energy range of $E_{\mathrm{c.m.}}$ = 470–670 keV.

Later, Couture et al. [10] from the University of Notre Dame developed a Q-value gating technique for measurement optimization with NaI and HPGe detectors. The NaI array was used to detect the high-energy primary transition to the 1.634-MeV first excited state of ^{20}Ne, and the HPGe detector was used to detect the deexcited 1.634-MeV γ-rays (see Fig. 1). A sum energy gate of ≥ 10 MeV was applied to

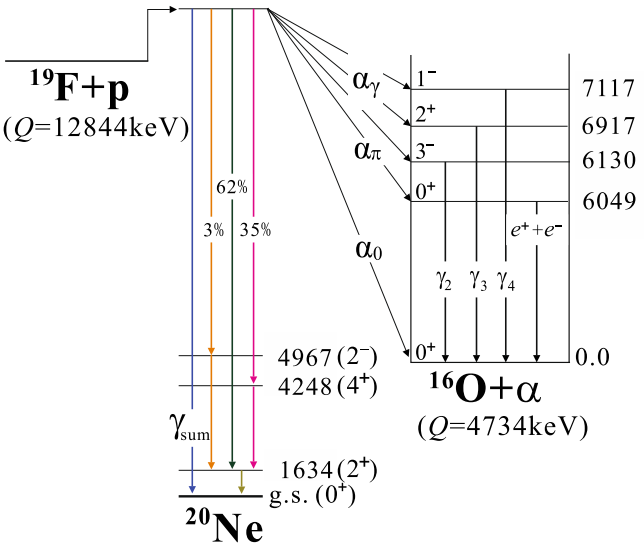

Fig. 1 Level scheme of the ^{19}F + p system [22]. The relevant γ-ray transitions are illustrated by the colored arrows. The transition branching ratios indicated refer to the $E_{\mathrm{c.m.}}$ = 225.2 keV resonance (corresponding to the values listed in Table 1). The transition to the ground state is referred to as (p, γ_0) (not labeled in the figure, but has the same energy with γ_{sum}), whereas all other transitions via the 1.634-MeV first excited state to the ground state are referred to as (p, γ_1). Here, γ_{sum} corresponds to the (~ 13-MeV peak in the 'sum' spectrum, and other transitions correspond to the peaks in the gated 'single' spectrum

filter out most of the 6–7 MeV γ-rays from the concurrent (p, $\alpha\gamma$) reactions. It is important to note that this technique is only sensitive to 1.634-MeV first excited state transitions; therefore, no direct transitions to the ground state of ^{20}Ne were measured. The ^{19}F(p, γ_1)^{20}Ne reaction was measured to be as low as $E_{\mathrm{c.m.}} \approx 220$ keV, but only the upper limits were given below $E_{\mathrm{c.m.}} \approx 300$ keV, which is still very far from the $E_{\mathrm{c.m.}} = 76$–148 keV Gamow window of primordial stars.

The latest measurement by Williams et al. [20] was performed using the inverse kinematics technique at TRIUMF. This work focused on the $E_{\mathrm{c.m.}} = 323$ keV resonance. A coincidence measurement of ^{20}Ne recoils and scattered γ-rays was used to suppress the high-intensity γ-ray background of the ^{19}F(p, $\alpha\gamma$)^{16}O reaction. The resonance branching ratio was determined for the first time in this study. The resonance strength was newly determined as $\omega\gamma = 3.0^{+1.1}_{-0.9}$ MeV, much larger than Couture et al.'s value [10], as the ground transition was also found to make a significant contribution in that work.

deBoer et al. [21] summarized all the available experimental data of the ^{19}F + p system and performed a comprehensive R-matrix analysis to obtain newly evaluated ^{19}F(p, γ)^{20}Ne and ^{19}F(p, α)^{16}O rates. Their (p, γ)/(p, α) rate ratio was approximately four times lower than that of a previous NACRE estimation [11]. This smaller ratio reduces the mass fractions of $Z > 9$ elements in the hydrogen-burning process of massive Pop III stars and intensifies the Ca production problem [21]. Furthermore, the estimated uncertainty of the ^{19}F(p, γ)^{20}Ne rate below 0.1 GK was as large as two orders of magnitude due to the lack of experimental data below 300 keV. This highlights the need for measuring the ^{19}F(p, γ)^{20}Ne reaction at low energies. In the present experiment, this break-out reaction was directly measured in the energy region $E_{\mathrm{c.m.}} = 186$–332 keV, which is the lowest energy region achieved to date. The brief results have been published elsewhere [22]. Here, we report the full experimental results, including the detailed γ-ray spectra and branching ratios, the contribution of the previously expected 212.7-keV resonance, and plans for future work.

2 Experiment

The China Jinping underground laboratory (CJPL) [23] is located in the traffic tunnel of a hydropower station under Jinping Mountain, with a vertical marble rock overburden of approximately 2400 m. The CJPL is currently the deepest operational underground laboratory for particle and nuclear physics experiments worldwide. The cosmic-ray-induced background measured at the CJPL [24] was approximately two orders of magnitude lower than that of LUNA (1400-m-thick dolomite rocks) in Italy [25]. Therefore, Jinping Underground laboratory for Nuclear Astrophysics (JUNA) [26] has been increasingly promoted owing to its unique extra-low-background environment [27]. At JUNA, we successfully conducted a ^{19}F(p, $\alpha\gamma$)^{16}O direct measurement campaign [13, 28] as a day-one experiment [29–34].

This ^{19}F(p, γ)^{20}Ne experiment was also conducted on the high-current 400-kV JUNA accelerator [35] at CJPL. A detailed diagram of the JUNA platform and the experimental setup is shown in Fig. 2. A proton beam from the accelerator was collimated by two apertures (ϕ15 mm upstream and ϕ12 mm downstream) and then impinged on a water-cooled target with a spot size of approximately 10 mm in diameter. For low-energy measurements away from the $E_{\mathrm{c.m.}} = 323.9$ keV resonance, where the cross section was low and a high-intensity beam was used ($I \approx 1$ mA), the beam was undulated periodically over the target surface

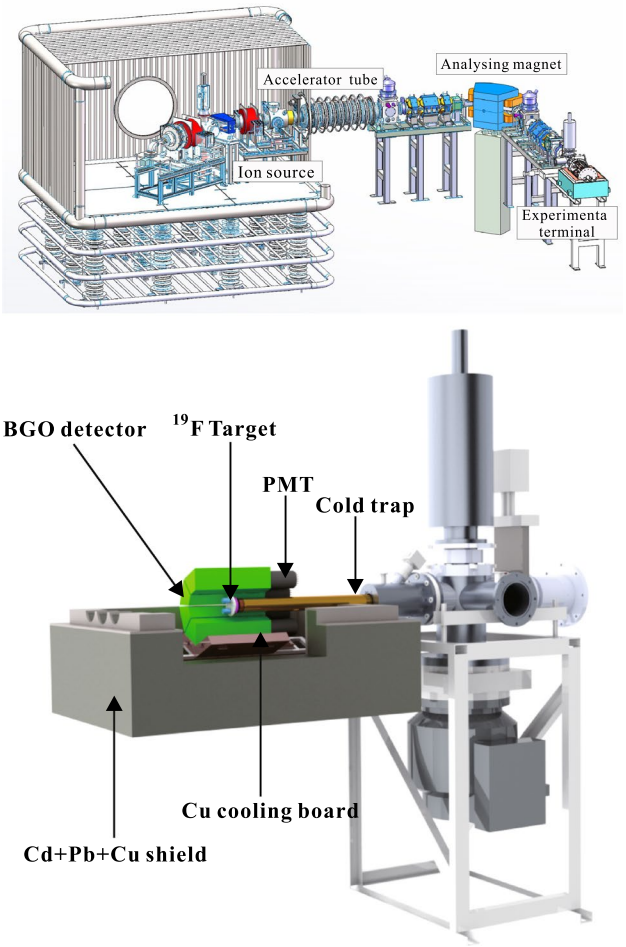

Fig. 2 (Color online) 3D schematic of the JUNA platform (upper panel) and experimental setup (lower panel) [22]. In the lower panel, the proton beam came in from the right side, passed through a cold trap, and impinged on the fluorine target. The γ-rays emitted were detected by a near 4π BGO detector array composed of eight identical segments. The BGO array was shielded by 5-mm Cu, 100-mm Pb, and 1-mm Cd layers from inside to outside [31]

to reduce target damage. However, because of the limited space, a beam raster was not installed in the first-stage JUNA experiments. Alternatively, the beam was scanned by periodically changing the magnetic field of the beam deflector installed approximately 3 m upstream of the target. Accordingly, the intense beam was spread over a rectangular area of approximately 40 mm × 40 mm. For the energy region close to the 323.9-keV resonance, the beam current was reduced to 1–10 μA to reduce the pileup of those strong 6130-keV γ rays from the ^{19}F(p, $\alpha\gamma_2$)^{16}O channel (see Fig. 1), and a beam-scanning system was not used. An inline Cu shroud cooled to the LN_2 temperature was extended close to the target to minimize carbon buildup on the target surface. There was no sign of carbon buildup upon visual inspection of any of the targets during the experiment. Together with the target, the Cu shroud constituted a Faraday cup for beam charge integration. A negative voltage of 300 V was applied to the shroud to suppress the secondary electrons from the target. The beam current error was estimated to be 1%, mainly because of Faraday cup leakage (typically < 10 nA) [36, 37]. Two strong and durable implanted ^{19}F targets developed in recent years were used in this study. The targets were fabricated by implanting 40 keV ^{19}F ions into 3-mm-thick high-purity Fe backing and then sputtering approximately 50-nm-thick Cr foils to further prevent fluorine material loss (see Refs. [38, 39]. The target characteristics were monitored by scanning the yield of the $E_{c.m.}$ = 323.9 keV resonance attributed to the (p, $\alpha\gamma$) channel (see Refs. [13, 22, 39] for details). The ^{19}F target used for the ^{19}F(p, γ) measurement was similar to that used in Ref. [36]. The target characterization is shown in Fig. 5 in Ref. [36]. In the present experiment, the target endured only 40 C bombardment and could therefore be considered stable.

A 4π BGO detector array specially designed for the JUNA project [26], which has already been used and characterized in previous studies [13, 22, 30, 31]), was used for γ-ray detection. The BGO array was composed of eight identical segments with a length of 250 mm and radial thickness of 63 mm, each covering a 45° azimuthal angle. For the 1634-keV γ-rays of interest, the coincidence efficiency was ≈ 14%, with an ≈ 10% energy resolution achieved via alcohol cooling of the BGO crystals (≈ 5 °C). To suppress the natural γ-ray background emitted from the rocks and induced by the neutron capture reactions on the material around the detector (e.g., support structures and rocks), the BGO array was shielded with 5-mm copper, 100-mm lead, and 1-mm cadmium. A constant nitrogen gas flow was injected into the BGO array to eliminate radioactive radon gas and avoid vapor buildup on the cold BGO crystals. A detailed description of this BGO array can be found in Ref. [40].

The spectrum of the sum of the energies of all eight BGO segments (hereafter referred to as 'sum' spectrum) and the spectrum of the energy measured by each single segment (called 'single' spectrum) were obtained. Figure 3 shows seven typical γ-ray energy spectra obtained at beam energies of E_p = 210–362 keV. As in our previous work [13, 22], E_p denotes the proton beam energy before the Cr protective layer of the implanted fluorine target. The background peaks at 1460.8 keV (from ^{40}K) and 2614.5 keV (from ^{208}Tl), along with the 6130-keV peak from the ^{19}F(p, $\alpha\gamma_2$)^{16}O (i.e., the α_2 channel) reaction, were used for energy calibration. Due to the high efficiency of the BGO array, only full energy peaks were observed in the 'sum' spectrum, and the single and double escape contributions are almost negligible. In addition, we observed γ-rays induced by the ^{12}C, ^{13}C, and ^{11}B impurities from the target materials and beam apertures (see the lower panel in Fig. 3).

3 Results

The ^{19}F(p, γ)^{20}Ne reaction is mainly dominated by decay through the first excited state (i.e., (p, γ_1)) and the ground state (i.e., (p, γ_0)) transitions [10, 20]. Therefore, a coincidence gating technique [22, 30, 31] was developed to analyze the data. By gating the (~ 13,000-keV peak in the 'sum' spectrum (see Fig. 3), which corresponds to the total reaction energy (i.e., Q-value plus incident energy), the 1634-keV peak can be clearly seen in the 'single' spectrum. As opposed to the 'sum' peak, which represents the total reaction energy, this gated 'single' spectrum reflects more individual transitions due to the smaller azimuthal angles (45°) covered by each BGO segment. The count of this 1634-keV peak was analyzed and used to calculate the ^{19}F(p, γ_1)^{20}Ne contribution [22]. The gate ranges were adjusted for each energy point to minimize fitting errors. Moreover, the gated 'single' spectrum is very sensitive to the decay routines. By reproducing this gated spectrum using the Geant4 simulation [41], the relevant γ-transition branching ratios and coincidence efficiency were determined for each energy point. Besides, it is possible for the 1634-keV γ-ray to enter a single BGO crystal simultaneously with other cascade γ rays, which is known as the "summing effect". This results in the presence of a sum of two energies on the 'single' spectrum, which affects the true counts of the 1634-keV γ-ray. For the 'single' spectrum with E_p = 250 keV, the summing effect accounted for approximately 16%. This effect is considered in Geant4 when calculating the absolute efficiency. The (~ 13,000-keV peak in the 'sum' spectrum includes the contributions from both the (p, γ_0) and (p, γ_1) branches. The (p, γ_0) branch yields were determined by subtracting the (p, γ_1) contribution determined above from the sum of the (~ 13,000-keV peak, that is, (p, γ_{tot}), after correcting for the respective energy-dependent efficiency values. The experimental data for the (p, γ_0) and (p, γ_1) yields

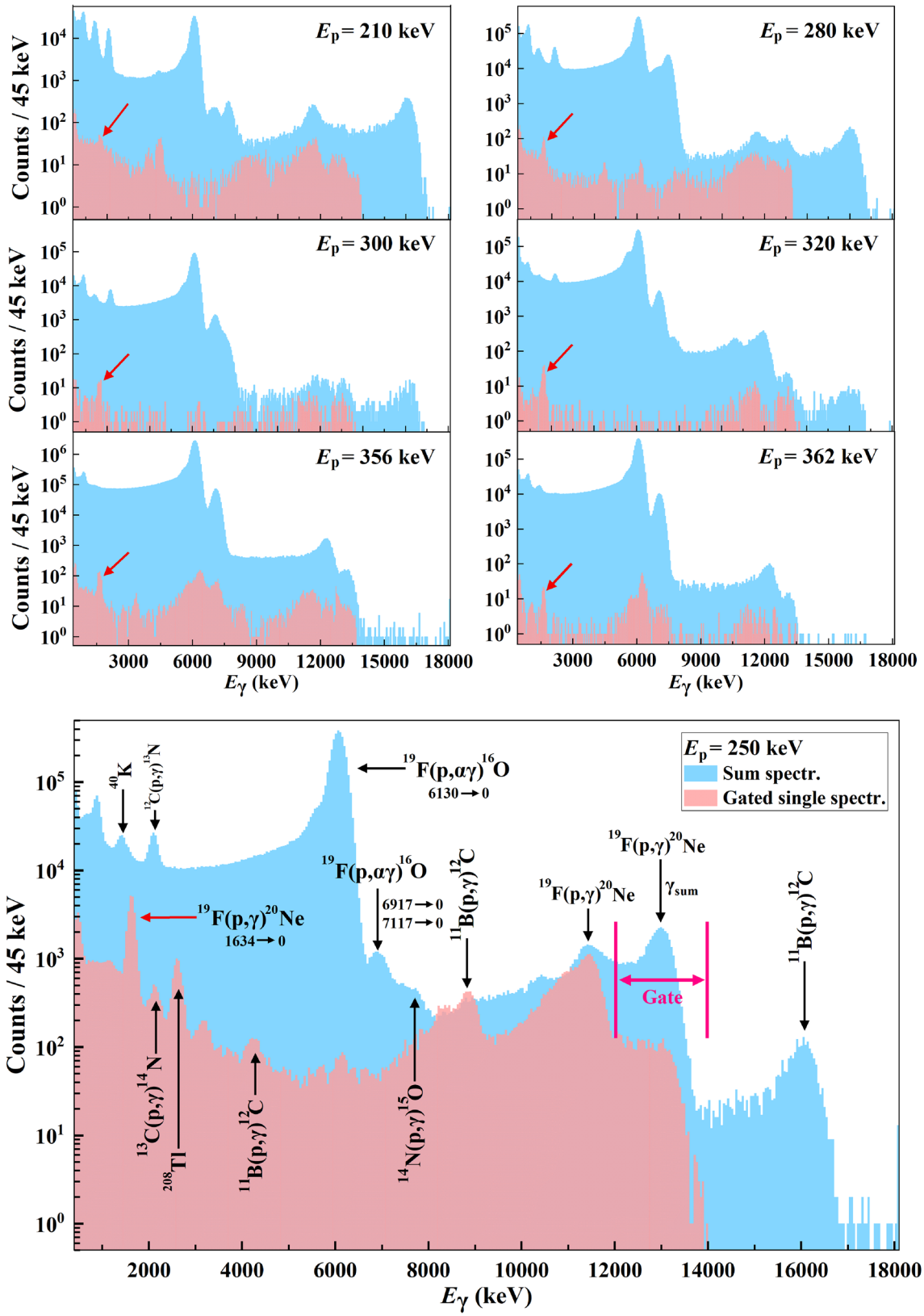

Fig. 3 (Color online) (Upper panel) Sample γ-ray spectra taken at beam energies of E_p = 210–362 keV. The red arrows indicate the 1634-keV peak, which corresponds to the γ transition from the first excited state to the ground state in ^{20}Ne. (Lower panel) Enlarged spectrum taken at a beam energy of E_p = 250 keV. The main background (from ^{40}K and ^{208}Tl) and the contaminant γ-ray peaks (i.e., from ^{12}C, ^{13}C, ^{11}B and ^{14}N) are explicitly indicated. All spectra have a bin width of 45 keV

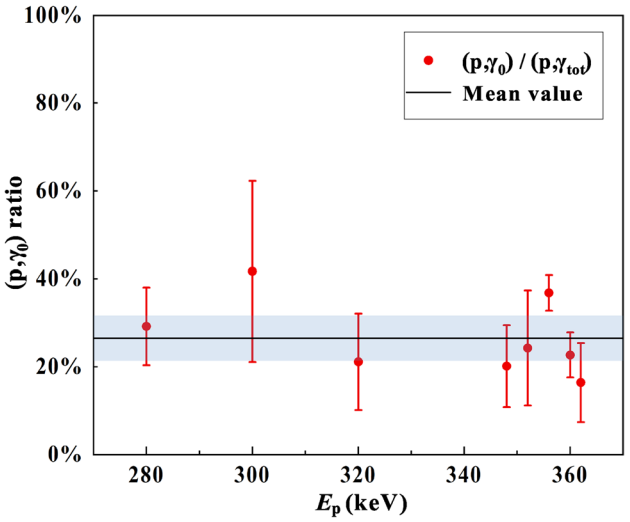

Fig. 4 Yield ratio of the (p,γ_0) branch to the total one (p,γ_0) + (p,γ_1). Here, the error bars shown represent only the statistical error; the black line and shadowed area represent the mean value (26.5%) and total error (5.2%), respectively

are reported in Ref. [22]. Figure 4 shows the yield ratios of (p, γ_0) and (p, γ_{tot}) obtained in the energy region of E_p = 280–360 keV. Here, the error bars indicate statistical significance. In general, this ratio is constant at ≈ 26.5%, as indicated by the solid line in Fig. 4. In other words, the (p, γ_1) branch dominated the entire energy region measured in this study, whereas the (p, γ_0) branch contributed only ≈ 26.5% over the energy region shown in the figure. The total ≈ 5.2% error band shown, including systematic and statistical errors, was calculated using Eq. 1. The systematic error comes mainly from the respective 11.5% and 4.7% relative errors of the (p, γ_1) and (p, γ_0) channels, which stems mainly from the detection efficiency uncertainty simulated by Geant4, which in turn results mainly from the uncertainty of the adopted branching ratio. The average statistical error of the eight data points shown in the figure is adopted as the statistical error (i.e., ≈ 3.97%). The coincidence efficiency was obtained through Geant4 simulations, which were verified using two standard ^{60}Co and ^{137}Cs sources. The uncertainty of the γ-ray energy difference in the Geant4 simulations between the radioactive sources and the (p, γ_1) reaction is far less than the branching ratio uncertainty. In addition, it should be noted that the (p, γ_0) contribution cannot be determined reliably for the two energy points at E_p = 210 and 220 keV because of serious ^{11}B contamination and the statistics; here, we roughly estimate its contribution at (~ 26%, which is consistent with the trend shown for the non-resonant-energy region (see Fig. 4). Furthermore, no noticeable (p, γ_0) contribution was observed over the newly observed resonance.

Table 1 γ-transition branching ratios obtained for the resonances at $E_{c.m.}$ = 225.2 and 323.9 keV

$E_r^{c.m.}$ (keV)	G.S	1.634 MeV	4.248 MeV	4.967 MeV
225.2	–	62%	35%	3%
323.9	34%	45%	–	21%

$$\begin{aligned} \mathrm{err}_{\mathrm{total}} &= \sqrt{\mathrm{err}_{\mathrm{sys.}}^2 + \mathrm{err}_{\mathrm{sta.}}^2} \\ &= \sqrt{(11.5\%^2 + 4.7\%^2) \times 26.5\%^2 + 3.97\%^2} \\ &\approx 5.2\% \end{aligned} \quad (1)$$

In this experiment [22], a key resonance was discovered at $E_{c.m.}$ = 225.2 keV in the (p, γ) channel for the first time. This corresponds to the E_x = 13.069 MeV (3^-) excited state in ^{20}Ne, which has already been observed in the (p, $\alpha\gamma$) channel [12, 13, 36, 39]. Its strength is determined by integrating its yield curve A_Y [42]:

$$A_Y = n\frac{\lambda_r^2}{2}\omega\gamma, \quad (2)$$

where λ_r is the de Broglie wavelength at the resonance energy, $\omega\gamma$ is the resonance strength, and n is the number of ^{19}F atoms in the target, which was determined by the resonance strength and yield integration (corrected for efficiency) of the well-studied 323.9-keV (p, $\alpha\gamma_2$) resonance and was determined to a precision of better than 4% [11, 13]. Therefore, the strength of this new resonance was determined as $\omega\gamma_{(p,\gamma_1)}$ = 41.9 ± 3.2(sys.) ± 0.1(sta.) μ eV [22]. Because its (p, γ_0) contribution is not significant, $\omega\gamma_{(p,\gamma_{tot})} \approx \omega\gamma_{(p,\gamma_1)}$ for this new resonance. Table 1 lists the related γ-transition branching ratios that were experimentally constrained for the first time in this study.

For the 323.9-keV (p, γ) resonance, only five energy points were measured owing to the limited beam time (see Fig. 1a in Ref. [22]), which is insufficient for obtaining a perfect yield curve. Instead, the (p, γ) strength was determined by directly comparing the corresponding (p, γ_1) and (p, γ_0) yields with the (p, $\alpha\gamma_2$) yields using Eq. 2. For the 323.9-keV resonance, three reaction channels—(p, γ_0), (p, γ_1), and (p, $\alpha\gamma_2$)—were measured at five energy points near the resonance. Therefore, the resonance strength ratio of these three channels is equal to the ratio of their γ-ray yields to the corrected detection efficiency. The (p, $\alpha\gamma$) strength was previously determined as $\omega\gamma_{(p,\alpha\gamma)}$ = (23.1 ± 0.9) eV [11]. Here, the (p, γ) strengths were determined to be $\omega\gamma_{(p,\gamma_1)}$=2.09 ± 0.16(sys.) ± 0.13(sta.) meV and $\omega\gamma_{(p,\gamma_0)}$=1.07 ± 0.08(sys.) ± 0.19(sta.) meV. Therefore, the total strength was determined as $\omega\gamma_{(p,\gamma_{tot})}$=3.16 ± 0.24(sys.) ± 0.23(sta.) me

V. The present $\omega\gamma_{(p,\gamma_1)}$ value roughly agrees with the previous value of (1.38 ± 0.44) meV [10] within the uncertainty range, but with much improved precision and with a higher central value. The present $\omega\gamma_{(p,\gamma_{tot})}$ value is consistent with the adopted value of (5 ± 3) meV [11], as well as with the recently reported value of $3.3^{+1.1}_{-0.9}$ meV [20] from TRIUMF, but with 4–7 times better precision.

Regarding the previously expected $E_{c.m.}$ = 212.7 keV (corresponding to the E_x = 13.056 MeV (2^-) excited state) resonance, which was always thought to dominate the (p, γ) reaction rate at low temperature below (~ 0.26 GK, the estimates placed the upper limits on its strength at 1.3 [11], 0.93 [10] and 0.83 μeV [21]. The contribution of this resonance was investigated by assuming different strengths relative to those of the 225.2-keV resonance, as shown in Fig. 5. Four strengths, 0%, 1%, 5%, and 10%, relative to that of $\omega\gamma^{225.2}_{(p,\gamma)}$ = 41.9 μeV, were investigated. This indicates that this resonance mainly increases the yield between E_p = 220–243 keV. Because of the limited beam time, we only measured one energy point in this range (E_p = 240 keV), which constrained the 212.7-keV strength to approximately 1% of the 225.2-keV resonance. To be conservative, we estimated the 212.7-keV strength to be < 4.2 μeV [22], that is, less than 10% of the 225-keV resonance.

For the non-resonant energy region, the product of the number of ^{19}F atoms and the absolute efficiency of the BGO detector was determined via the (p, $\alpha\gamma$) yield over the $E_{c.m.}$ = 323.9 keV resonance [22, 36]. Using this method, the astrophysical S-factors of the ^{19}F(p, γ)^{20}Ne reaction were calculated using this product and the γ-ray yields, as shown in Fig. 1b in Ref. [22]. The systematic uncertainty of the S-factors includes: (i) a 5% uncertainty estimated for the Geant4 simulation by assuming a 0.5-keV uncertainty in the reconstructed $E_{c.m.}$ energy; (ii) a 3.9% uncertainty of the 323-keV resonance strength (from the normalization); and (iii) a 5%–10% uncertainty of the 1634-keV γ -ray coincidence efficiency. From this, we conservatively estimate an overall systematic uncertainty of (~ 12%.

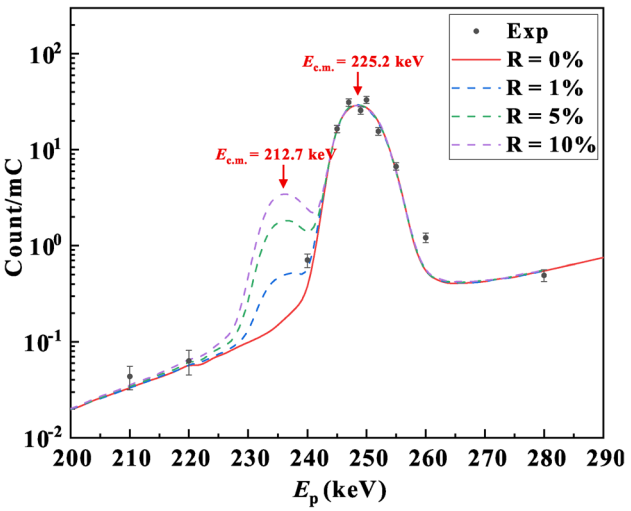

Fig. 5 Geant4 simulated influence of the previously expected $E_{c.m.}$ = 212.7 keV resonance to the measured (p, γ) yields. The legend "R" refers to the strength ratio of $\omega\gamma^{212.7}_{(p,\gamma)}$ / $\omega\gamma^{225.2}_{(p,\gamma)}$, e.g., R = 1% denotes a 212.7-keV resonance strength assumed to be 1% that of the 225.2-keV resonance

4 *R*-matrix analysis

A multi-level, multi-channel R-matrix analysis of the ^{20}Ne system near the proton separation energy [21] using the AZURE2 code [43] was used to reproduce the experimental data (see Fig. 7). Because of off-resonance data scarcity, owing to the limited beam time and the rather high-level density, which may not be fully known, there is some ambiguity regarding the underlying reaction components that produce a fairly constant S-factor at the lowest energies. For example, as shown in Fig. 7, the trend of the experimental data can be reproduced using the high-energy tail of either a very-low-energy resonance or a subthreshold resonance. Furthermore, the level density in this energy region is sufficiently high such that there are several subthreshold state candidates, any of which, or a combination thereof, can equally reproduce the observed energy dependence. Moreover, the total threshold resonance width has large uncertainties [12, 21]. If the width is near its upper limit, a high-energy tail can significantly enhance the low-energy S-factor.

Under the above assumptions, Bayesian uncertainty analysis (see Extended Data Fig. 4 in Ref. [22]) was performed using the Python package BRICK [44]. BRICK acts as a mediator, allowing communication between the Python MCMC sampler emcee [45] and the C++ R-matrix code AZURE2. This analysis was used to estimate the uncertainty of the low-energy S-factor.

The phenomenological R-matrix is not a predictive theory. Instead, it relies on a presupposed knowledge of the level structure. When this information is incomplete, it translates into large uncertainties that must be estimated based on the theoretical limits of the resonance parameters. While not indicated in Fig. 7, additional resonance contributions are possible given the high density of ^{20}Ne at these energies [46]. These resonances could be broad, corresponding to those observed in ^{16}O(α, α)^{16}O data [47, 48], but could also be narrow, such as the one reported here at 225.2 keV. If so, further enhancement of the S-factor would be possible; accordingly, further low-energy studies are highly encouraged.

5 Reaction rate

The astrophysical *S*-factors obtained by the *R*-matrix fitting were used to calculate the thermonuclear ^{19}F(p, γ)^{20}Ne reaction rate (see Fig. 2 in Ref. [22]), which is not repeated here. As discussed in the Introduction, the ratio of the ^{19}F(p, γ)^{20}Ne and ^{19}F(p, $\alpha\gamma$)^{16}O reaction rates influences Ca production in Population III stars. Figure 6 shows the corresponding rate ratios and associated uncertainties.

The mean value (solid line) and upper and lower limits (boundary of the colored band) were calculated using the *adopted*/*adopted*, *high*/*low*, and *low*/*high* combinations of the corresponding (p, γ) and (p, α) rates. At the hydrogen-burning temperature (~ 0.14 GK of first stars of interest, the (p, γ)/(p, α) ratio (mean value) is 8.7×10^{-4}, which is approximately 6.4 and 18.3 times larger than the NACRE [11] and deBoer et al. [21] estimations, respectively.

This significantly enhanced new ratio leads to a much stronger break-out from the CNO cycles to the heavier mass region, as far as the doubly magic isotope ^{40}Ca. Here, the typical temperature of these oldest stars is approximately four times warmer than that of modern massive stars, and may thus be considered as a "*warm*" CNO cycle (see the Supplemental Materials in Ref. [22]). Therefore, the observed Ca abundance in the oldest star known to date, SMSS0313-6708, can be reproduced using this new ratio (see Fig. 3 in Ref. [22]). Furthermore, ^{19}F(p, γ)^{20}Ne is the only reaction that can remove the catalytic material from the cycle at low temperatures, causing an irreversible flow from the CNO to the NeNa region, because back-processing via ^{22}Ne(p, α)^{19}F is not energetically possible. Thus, this break-out permanently removed the catalytic material from the CNO cycles and significantly changed the energy-production rate and stellar lifetime for hydrogen burning [5, 22].

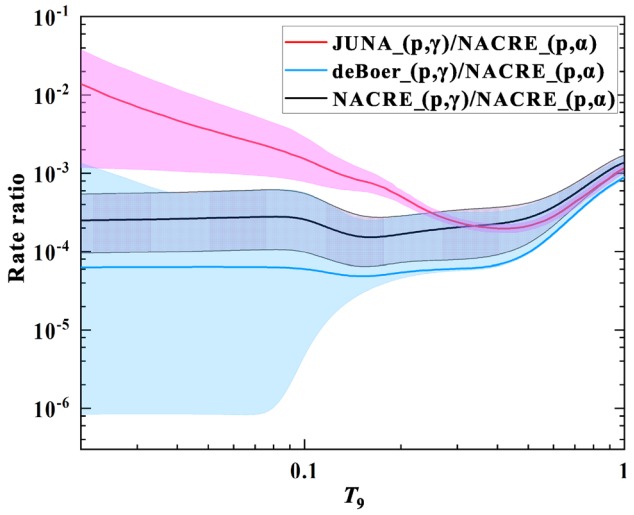

Fig. 6 (Color online) Ratio of ^{19}F(p, γ)^{20}Ne and ^{19}F(p, α)^{16}O thermonuclear rates. The mean value (solid line) and the upper and lower limits (boundary of the error band) were calculated by the *adopted*/*adopted*, *high*/*low*, and *low*/*high* combinations of the corresponding (p, γ) and (p, α) rates. Three (p, γ) rates, namely JUNA [22], deBoer et al. [21] and NACRE [11], are compared to the NACRE-recommended (p, α) rate. Here, T_9 represents the temperature in 10^9 kelvin (i.e., in gigakelvin, GK)

6 Summary

This paper reports the full experimental results for the astrophysical important ^{19}F(p, γ)^{20}Ne reaction. The measurement directly reached the lowest energy region of $E_{\mathrm{c.m.}} \approx 186$–$332$ keV, relying on the extra-low background deep underground environment, as well as the extensive proton beam from the JUNA facility. A gating technique was developed to determine the ^{19}F(p, γ)^{20}Ne yield. The astrophysical *S*-factors were obtained from an *R*-matrix analysis along with MCMC Bayesian uncertainty estimation. A new resonance

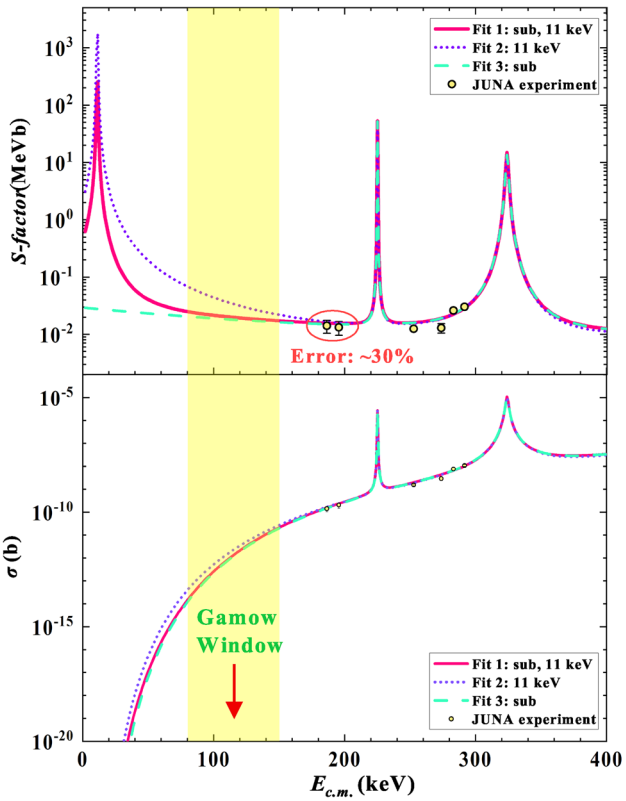

Fig. 7 (Color online) ^{19}F(p, γ_1)^{20}Ne astrophysical *S*-factors (upper panel, also see Fig. 1b in Ref. [22]) and cross section (lower panel). Where the statistical error of the two lowest energy points achieved at JUNA is ≈ 30% (shown within the red circle), and the three probable *R*-Matrix fitted curves shown can be used for low-energy extrapolation. The yellow shaded area indicates the typical Gamow window of Pop III stars in their hydrogen-burning stage

at $E_{\mathrm{c.m.}}$ = 225.2 keV was observed, and its resonance strength was precisely determined to be $\omega\gamma_{(\mathrm{p},\gamma_{\mathrm{tot}})} = \omega\gamma_{(\mathrm{p},\gamma_1)} = 41.9 \pm 3.2(\mathrm{sys}) \pm 0.1(\mathrm{sta})$ μeV. This resonance increases the (p, γ)/(p, α) ratio by a factor of 5.4–7.4 at a typical hydrogen-burning temperature of approximately 0.14 GK. This enhanced ratio causes a much stronger break-out from the "*warm*" CNO cycle scenario via the ^{19}F(p, γ)^{20}Ne, which significantly increases the production of Ne up through Ca nuclei. It is found that the observed Ca abundance of the oldest known ultra-iron-poor star (SMSS0313-6708) can be reproduced well with the new JUNA (p, γ) rate and thus may reveal the nature of Ca production in Pop III stars.

Figure 7 shows the present ^{19}F(p, γ_1)^{20}Ne astrophysical *S*-factors (upper panel) and cross-sections (lower panel), along with the three most probable *R*-matrix fitted curves [22]. The Gamow window shown for this break-out reaction is located at $E_{\mathrm{c.m.}} \approx (112 \pm 36)$ keV for the Pop III stars at their typical temperature of ≈ 0.1 GK. Because of the limited beam time, the present two lowest data (within the red circle) still have (∼ 30% statistical error, and the predicted *S*-factor uncertainty by the *R*-matrix fits is as large as a factor of approximately 1.8 at the Gamow peak. Therefore, it is necessary to measure this reaction directly down to the Gamow window. Thus, a reaction rate around 0.1 GK of astrophysical importance and the properties of the $E_{\mathrm{c.m.}} = 11$ keV near-threshold resonance can be constrained more strictly based on solid experimental ground.

It is expected that the cross section will exhibit an exponential decline with decreasing beam energy; for example, the cross section will decrease to 10^{-14} (∼ 10^{-11} b within the Gamow window; therefore, the ^{11}B contamination in the implanted ^{19}F target, with a much larger (p, γ) cross section, will become the main obstacle. Recently, we built a new target-making device on an electromagnetic isotope separator [49], in which a 180° analyzing magnet and an LN_2 cold trap were applied to reduce contamination during implantation. Moreover, to reduce boron contamination in the Fe backing, a high-purity Fe coating is now magnetron-sputtered onto the original Fe backing, and such an additional coating can effectively reduce boron contamination. Preliminary results show that ^{11}B contamination in new targets can be reduced by more than a factor of 10 [50].

In a future JUNA experiment, we will use the newly developed implanted targets and the new 4π BGO array to extend the ^{19}F(p, γ)^{20}Ne measurements directly to the Gamow window. Additional experimental data over the 212.7-keV resonance will be acquired to accurately characterize its strength. These precise experimental data will be very helpful for understanding the nucleosynthesis and evolution of first stars in our early Universe, as the observation of first stars is one of the key mission targets of the James Webb Space Telescope (JWST) [51]. Furthermore, as shown in Fig. 6, the present (p, γ)/(p, α) rate ratio is approximately 200 times larger than the NACRE estimation at temperatures of approximately 0.01 GK. This strikingly enhanced break-out may have important astrophysical implications, and the impact of our reported rate on novae, X-ray bursts, asymptotic giant branch (AGB) stars, and other stellar sites is still the subject of future research.

Author Contributions All authors contributed to the study conception and design. Material preparation, data collection and analysis were performed by Yin-Ji Chen, Li-Yong Zhang, Hao Zhang, Jian-Jun He, R. J. deBoer. The first draft of the manuscript was written by Yin-Ji Chen and all authors commented on previous versions of the manuscript. All authors read and approved the final manuscript.

Data availability The data that support the findings of this study are openly available in Science Data Bank at https://cstr.cn/31253.11.sciencedb.j00186.00197 and https://www.doi.org/10.57760/sciencedb.j00186.00197.

Declarations

Conflict of interest The authors declare that they have no conflict of interest.

References

1. V. Bromm, R.B. Larson, The first stars. Annu. Rev. Astron. Astron. **42**, 79 (2004). https://doi.org/10.1146/annurev.astro.42.053102.134034
2. C.E. Rolfs, W.S. Rodney, *Cauldrons in the Cosmos* (University of Chicago Press, Chicago, 1988)
3. E.G. Adelberger, A. Garciá, H.R.G. Robertson et al., Solar fusion cross sections. II. The pp chain and CNO cycles. Rev. Mod. Phys. **83**, 195–245 (2011). https://doi.org/10.1103/RevModPhys.83.195
4. M. Wiescher, O. Clarkson, R.J. de Boer et al., Nuclear clusters as the first stepping stones for the chemical evolution of the universe. Eur. Phys. J. A **57**, 24 (2021). https://doi.org/10.1140/epja/s10050-020-00339-x
5. M. Wiescher, J. Görres, H. Schatz, Break-out reactions from the CNO cycles. J. Phys. G **25**, R133–R161 (1999). https://doi.org/10.1088/0954-3899/25/6/201
6. S.C. Keller, M.S. Bessell, A. Frebel et al., A single low-energy, iron-poor supernova as the source of metals in the star SMSS J031300.36–670839.3. Nature **506**, 463–466 (2014). https://doi.org/10.1038/nature12990
7. O. Clarkson, F. Herwig, Convective H-He interactions in massive population III stellar evolution models. Mon. Not. R. Astron. Soc. **500**, 2685–2703 (2021). https://doi.org/10.1093/mnras/staa3328
8. K. Takahashi, H. Umeda, T. Yoshida, Stellar yields of rotating first stars. I. Yields of weak supernovae and abundances of carbon-enhanced hyper-metal-poor stars. Astrophys. J. **794**, 40 (2014). https://doi.org/10.1088/0004-637X/794/1/40
9. M. Arnould, N. Mowlavi, A.E. Champagne, Non-explosive hydrogen burning: Where do we stand? 32nd Liège Inter. Astrophys. Coll. (1995). http://www.ago.ulg.ac.be/PeM/Coll/Liac32/
10. A. Couture, M. Beard, M. Couder et al., Measurement of the ^{19}F(p, γ)^{20}Ne reaction and interference terms from $E_{\mathrm{c.m.}}$=200–760 keV. Phys. Rev. C **77**, 015802 (2008). https://doi.org/10.1103/PhysRevC.77.015802

11. C. Angulo, M. Arnould, M. Rayet et al., A compilation of charged-particle induced thermonuclear reaction rates. Nucl. Phys. A **656**, 3 (1999). https://doi.org/10.1016/S0375-9474(99)00030-5
12. K. Spyrou, C. Chronidou, S. Harissopulos et al., Cross section and resonance strength measurements of ^{19}F(p, $\alpha\gamma$)^{16}O at E_p= 200–800 keV. Eur. Phys. J. A **7**, 79–85 (2000). https://doi.org/10.1007/s100500050014
13. L.Y. Zhang, J. Su, J.J. He et al., Direct measurement of the astrophysical ^{19}F(p, $\alpha\gamma$)^{16}O reaction in the deepest operational underground laboratory. Phys. Rev. Lett. **127**, 152702 (2021). https://doi.org/10.1103/PhysRevLett.127.152702
14. L. Keszthelyi, I. Berkes, I. Demeter et al., Resonances in ^{19}F+p reactions at 224 and 340 keV proton energies. Nucl. Phys. **29**, 241–251 (1962). https://doi.org/10.1016/0029-5582(62)90177-3
15. I. Berkes, I. Dezsi, I. Fodor et al., The resonance at 483 and 597 keV proton energies in ^{19}F+p reactions. Nucl. Phys. **43**, 103–109 (1963). https://doi.org/10.1016/0029-5582(63)90332-8
16. G.K. Farney, H.H. Givin, B.D. Kern et al., High-energy gamma rays from the proton bombardment of fluorine. Phys. Rev. **97**, 720–725 (1955). https://doi.org/10.1103/PhysRev.97.72
17. R.M. Sinclaii, Gamma radiation from certain nuclear reactions. Phys. Rev. **93**, 1082–1086 (1954). https://doi.org/10.1103/PhysRev.93.1082
18. K.M. Subotić, R. Ostogić, B.Z. Stepančić, Study of the ^{19}F(p, γ)^{20}Ne radiative capture reaction from 0.2–1.2 MeV. Nucl. Phys. A **331**, 491–501 (1979). https://doi.org/10.1016/0375-9474(79)90355-5
19. E.T. Clifford, Master's thesis, University of Toronto (1974)
20. M. Williams, P. Adsley, B. Davids et al., New measurement of the E_{cm}=323 keV resonance in the ^{19}F(p, γ)^{20}Ne reaction. Phys. Rev. C **103**, 055805 (2021). https://doi.org/10.1103/PhysRevC.103.055805
21. R.J. deBoer, O. Clarkson, A.J. Couture et al., ^{19}F(p, γ)^{20}Ne and ^{19}F(p, α)^{16}O reaction rates and their effect on calcium production in Population III stars from hot CNO breakout. Phys. Rev. C **103**, 055815 (2021). https://doi.org/10.1103/PhysRevC.103.055815
22. L.Y. Zhang, J.J. He, R.J. de Boer et al., Measurement of ^{19}F(p, γ)^{20}Ne reaction suggests CNO breakout in first stars. Nature **610**, 656–660 (2022). https://doi.org/10.1038/s41586-022-05230-x
23. K.J. Kang, J.P. Cheng, Y.H. Chen et al., Status and prospects of a deep underground laboratory in China. J. Phys. Conf. Ser. **203**, 012028 (2010). https://doi.org/10.1088/1742-6596/203/1/012028
24. Y.C. Wu, X.Q. Hao, Q. Yue et al., Measurement of cosmic ray flux in the China JinPing underground laboratory. Chin. Phys. C **37**, 086001 (2013). https://doi.org/10.1088/1674-1137/37/8/086001
25. C. Broggini, D. Bemmerer, A. Guglielmetti et al., LUNA: nuclear astrophysics deep underground. Annu. Rev. Nucl. Part. Sci. **60**, 53 (2010). https://doi.org/10.1146/annurev.nucl.012809.104526
26. W.P. Liu, Z.H. Li, J.J. He et al., Progress of Jinping underground laboratory for nuclear astrophysics (JUNA). Sci. China-Phys. Mech. Astron. **59**, 642001 (2016). https://doi.org/10.1007/s11433-016-5785-9
27. Y.P. Shen, J. Su, W.P. Liu et al., Measurement of γ detector backgrounds in the energy range of 3–8 MeV at Jinping underground laboratory for nuclear astrophysics. Sci. China-Phys. Mech. Astron. **60**, 102022 (2017). https://doi.org/10.1007/s11433-017-9049-3
28. J.J. He, S.W. Xu, S.B. Ma et al., A proposed direct measurement of cross section at Gamow window for key reaction ^{19}F(p, α)^{16}O in Asymptotic Giant Branch stars with a planned accelerator in CJPL. Sci. China-Phys. Mech. Astron. **59**, 652001 (2016). https://doi.org/10.1007/s11433-016-5797-5
29. Y.J. Chen, L.Y. Zhang, Examining the fluorine overabundance problem by conducting Jinping deep underground experiment. Nuclear Techniques **46**, 110501 (2023). https://doi.org/10.11889/j.0253-3219.2023.hjs.46.110501. (**in Chinese**)
30. L.H. Wang, J. Su, Y.P. Shen et al., Measurement of the ^{18}O(α, γ)^{22}Ne reaction rate at JUNA and its impact on probing the origin of SiC grains. Phys. Rev. Lett. **130**, 092701 (2023). https://doi.org/10.1103/PhysRevLett.130.092701
31. J. Su, H. Zhang, Z.H. Li et al., First result from the Jinping underground nuclear astrophysics experiment JUNA: precise measurement of the 92 keV ^{25}Mg(p, γ)^{26}Al resonance. Sci. Bull. **67**, 125–132 (2022). https://doi.org/10.1016/j.scib.2021.10.018
32. B. Gao et al., Deep underground laboratory measurement of ^{13}C(α, n)^{16}O in the Gamow windows of the *s* and *i* processes. Phys. Rev. Lett. **129**, 132701 (2022). https://doi.org/10.1103/PhysRevLett.129.132701
33. T. Kajino, Underground laboratory JUNA shedding light on stellar nucleosynthesis. Nucl. Sci. Tech. **34**, 42 (2023). https://doi.org/10.1007/s41365-023-01196-1
34. C. Chen, Y.J. Li, Preparation of large-area isotopic magnesium targets for the ^{25}Mg(p,γ)^{26}Al experiment at JUNA. Nucl. Sci. Tech. **31**, 91 (2020). https://doi.org/10.1007/s41365-020-00800-y
35. Q. Wu, L.T. Sun, B.Q. Cui et al., Design of an intense ion source and LEBT for Jinping underground nuclear astrophysics experiments. Nucl. Instrum. Meth. A **830**, 214–218 (2016). https://doi.org/10.1016/j.nima.2016.05.099
36. L.Y. Zhang, J. Su, J.J. He et al., Direct measurement of the astrophysical ^{19}F(p, $\alpha\gamma$)^{16}O reaction in a deep-underground laboratory. Phys. Rev. C **106**, 055803 (2022). https://doi.org/10.1103/PhysRevC.106.055803
37. E.D. Cantero, A. Sosa, W. Andreazza, Design of a compact Faraday cup for low energy, low intensity ion beams. Nucl. Instrum. Meth. A **807**, 86–93 (2016). https://doi.org/10.1016/j.nima.2015.09.096
38. L.Y. Zhang, S.W. Xu, J.J. He et al., Properties of fluorine targets and their application on the astrophysically important ^{19}F(p, α)^{16}O reaction. Nucl. Instrum. Meth. B **438**, 48–53 (2019). https://doi.org/10.1016/j.nimb.2018.10.024
39. L.Y. Zhang, Y.J. Chen, J.J. He et al., Strong and durable fluorine-implanted targets developed for deep underground nuclear astrophysical experiments. Nucl. Instrum. Meth. B **496**, 9–15 (2021). https://doi.org/10.1016/j.nimb.2021.03.017
40. H. Zhang, J. Su, Z.H. Li et al., Nucl. Instrum. Meth. A, to be submitted
41. S. Agostinelli, J. Allison, K. Amako et al., Geant4: a simulation toolkit. Nucl. Instrum. Meth. A **506**, 250–303 (2003). https://doi.org/10.1016/S0168-9002(03)01368-8
42. C. Iliadis, *Nuclear Physics of Stars* (Wiley Verlag GmbH Co, KGaA, 2007)
43. R.E. Azuma, E. Uberseder, E. Simpson et al., AZURE: an R-matrix code for nuclear astrophysics. Phys. Rev. C **81**, 045805 (2010). https://doi.org/10.1103/PhysRevC.81.045805
44. D. Odell, C. Brune, D. Phillips et al., Performing Bayesian analysis with `AZURE2` using `BRICK`: an application to the ^{7}BRICKe system, Pip install Brick–James (unpublished)
45. D. Foreman-Mackey, D.W. Hogg, D. Lang et al., emcee: the MCMC hammer. Publ. Astron. Soc. Pac. **125**, 306–312 (2013). https://doi.org/10.1086/670067
46. D.R. Tilley, C.M. Cheves, J.H. Kelley et al., Energy levels of light nuclei, A = 20. Nucl. Phys. A **636**, 249–364 (1998). https://doi.org/10.1016/S0375-9474(98)00129-8
47. G. Caskey, Natural parity states of ^{20}Ne for $12 < E_x < 15.5$ MeV. Phys. Rev. C **31**, 717–735 (1985). https://doi.org/10.1103/PhysRevC.31.717
48. M.K. Mehta, W.E. Hunt, R.H. Davis, Scattering of alpha particles by oxygen. II. Bombarding energy range 10 to 19 MeV. Phys. Rev. **160**, 791–802 (1967)
49. Y.G. Liu, Q. Wu, X. Zhang et al., Design of a 180° electromagnetic isotope separator with inhomogeneous magnetic field. Nucl.

Instrum. Meth. A **1006**, 165428 (2021). https://doi.org/10.1016/j.nima.2021.165428
50. H. Zhang et al., Nucl. Instr. Meth. B, to be submitted
51. A. Witze, The $11-billion Webb telescope aims to probe the early Universe. Nature **600**, 208–212 (2021). https://doi.org/10.1038/d41586-021-03620-1

Authors and Affiliations

Yin-Ji Chen[1] · Hao Zhang[1] · Li-Yong Zhang[1,11] · Jian-Jun He[1,12] · Richard James deBoer[2] · Michael Wiescher[2] · Alexander Heger[3] · David Kahl[4] · Jun Su[1,11] · Daniel Odell[5] · Xin-Yue Li[1] · Jian-Guo Wang[6] · Long Zhang[7] · Fu-Qiang Cao[7] · Zhi-Cheng Zhang[8] · Xin-Zhi Jiang[1] · Luo-Huan Wang[1,13] · Zi-Ming Li[1] · Lu-Yang Song[1] · Liang-Ting Sun[6,9] · Qi Wu[6] · Jia-Qing Li[6] · Bao-Qun Cui[7] · Li-Hua Chen[7] · Rui-Gang Ma[7] · Er-Tao Li[8] · Gang Lian[7] · Yao-De Sheng[1] · Zhi-Hong Li[7] · Bing Guo[7] · Wei-Ping Liu[7,10]

✉ Li-Yong Zhang
liyongzhang@bnu.edu.cn

✉ Richard James deBoer
rdeboer1@nd.edu

✉ Wei-Ping Liu
wpliu@sustech.edu.cn

1 Key Laboratory of Beam Technology of the Ministry of Education, College of Nuclear Science and Technology, Beijing Normal University, Beijing 100875, China

2 Department of Physics and Astronomy, The Joint Institute for Nuclear Astrophysics, University of Notre Dame, Notre Dame, IN 46556, USA

3 School of Physics and Astronomy, Monash University, Clayton, VIC 3800, Australia

4 Facility for Rare Isotope Beams, Michigan State University, East Lansing, MI 48824, USA

5 Institute of Nuclear and Particle Physics and Department of Physics and Astronomy, Ohio University, Athens, OH 45701, USA

6 Institute of Modern Physics, Chinese Academy of Sciences, Lanzhou 730000, China

7 China Institute of Atomic Energy, Beijing 102413, China

8 College of Physics and Optoelectronic Engineering, Shenzhen University, Shenzhen 518060, China

9 School of Nuclear Science and Technology, University of Chinese Academy of Sciences, Beijing 100049, China

10 College of Science, Southern University of Science and Technology, Shenzhen 518055, China

11 Institute of Radiation Technology, Beijing Academy of Science and Technology, Beijing 100875, China

12 Key Laboratory of Nuclear Physics and Ion-Beam Application (MOE), Institute of Modern Physics, Fudan University, Shanghai 200433, China

13 School of Mathematics and Physics, Handan University, Handan 056005, China